Revisiting the reaction of dicarbonyls in aerosol proxy solutions containing ammonia: the case of butenedial

Jack C. Hensley[1], Adam W. Birdsall[2,a], Gregory Valtierra[3], Joshua L. Cox[2], Frank N. Keutsch[1,2,4]

[1]School of Engineering and Applied Sciences, Harvard University, Cambridge, MA, USA
[2]Department of Chemistry and Chemical Biology, Harvard University, Cambridge, MA, USA
[3]Harvard College, Cambridge, MA, USA
[4]Department of Earth and Planetary Sciences, Harvard University, Cambridge, MA, USA
[a]now at: Goodyear, Akron, OH, USA

Correspondence to: Jack C. Hensley (jhensley@g.harvard.edu) and Frank N. Keutsch (keutsch@seas.harvard.edu)

Abstract. Reactions in aqueous solutions containing dicarbonyls (especially the α-dicarbonyls methylglyoxal, glyoxal, and biacetyl) and reduced nitrogen (NH_X) have been studied extensively. It has been proposed that accretion reactions from dicarbonyls and NH_X could be a source of particulate matter and brown carbon in the atmosphere and therefore have direct implications for human health and climate. Other dicarbonyls, such as the 1,4-unsaturated dialdehyde butenedial, are also produced from the atmospheric oxidation of volatile organic compounds, especially aromatics and furans, but their aqueous phase reactions with NH_X have not been characterized. In this work, we determine a pH-dependent mechanism of butenedial reactions in aqueous solutions with NH_X that is compared to α-dicarbonyls, in particular the dialdehyde glyoxal. Similar to glyoxal, butenedial is strongly hydrated in aqueous solutions. Butenedial reaction with NH_X also produces nitrogen-containing rings and leads to accretion reactions that form brown carbon. Despite glyoxal and butenedial both being dialdehydes, butenedial is observed to have three significant differences in its chemical behavior: (1) as previously shown, butenedial does not substantially form acetal oligomers, (2) the butenedial/OH^- reaction leads to light-absorbing compounds, and (3) the butenedial/NH_X reaction is fast and first order in the dialdehyde. Building off of a complementary study on butenedial gas-particle partitioning, we suggest that the behavior of other reactive dialdehydes and dicarbonyls may not always be adequately predicted by α-dicarbonyls, even though their dominant functionalities are closely related. The carbon skeleton (e.g., its hydrophobicity, length, and bond structure) also governs the fate and climate-relevant properties of dicarbonyls in the atmosphere. If other dicarbonyls behave like butenedial, their reaction with NH_X could constitute a regional source of brown carbon to the atmosphere.

1 Introduction

Atmospheric particles are known to contain organic compounds that absorb light (Andreae and Gelencser, 2006; Bond et al., 2007; Laskin et al., 2015). One source of this so-called "brown carbon" is the irreversible reaction between dicarbonyls and reduced nitrogen (NH_X, here $NH_X = NH_3 + NH_4^+$) that takes place in the aqueous phase of atmospheric particles and in cloud

droplets (Debus, 1858; Loeffler et al., 2006; McNeill, 2015; Nozière et al., 2007; Volkamer et al., 2007). Because the ensuing accretion reactions form low-volatility products that tend to remain in the particle phase, brown carbon chemistry increases both the loading of atmospheric particles and their capacity to absorb light. Thus, aqueous-phase dicarbonyl/NH$_X$ reactions in the atmosphere have direct implications for human health and climate (Kanakidou et al., 2005; Pöschl, 2005).

35   Members of the dicarbonyl family are characterized by their dominant functionality, which is the identity of their two carbonyls. Dicarbonyls are either diketones, e.g., biacetyl, dialdehydes, e.g., glyoxal and butenedial, or ketoaldehydes, e.g., methylglyoxal. The number of aldehydes versus ketones has a strong influence on chemical reactivity. Atmospheric dicarbonyls can have long or short carbon backbones that are saturated or unsaturated (Bierbach et al., 1994; Obermeyer et al., 2009). The most measured and studied dicarbonyls in the atmosphere are the α-dicarbonyls, in particular glyoxal (C$_2$H$_2$O$_2$)

40 and methylglyoxal (C$_3$H$_4$O$_2$), which are the smallest dialdehyde and ketoaldehyde, respectively. Recently, biacetyl (C$_4$H$_6$O$_2$), the smallest diketone, has also received scientific attention (Grace et al., 2020; Kampf et al., 2016). Larger, complex dicarbonyls are also thought to be important products of biomass burning and fossil fuel combustion (Arey et al., 2009; Aschmann et al., 2011, 2014; Gómez Alvarez et al., 2007, 2009; Volkamer et al., 2001; Yuan et al., 2017), but they have rarely been studied or quantified in the atmosphere. Challenges include their high reactivity, no commercial availability, and

45 difficulties in analysis via chromatography (Hamilton et al., 2003; Smith et al., 1999). However, if the dominant functionality governs chemical behavior, then the well-understood α-dicarbonyls can "stand in" for others from the larger compound class, but it is important to evaluate the limitations of this approach.

      Quantitative understanding of dicarbonyl/NH$_X$ chemistry has come from laboratory studies of glyoxal, methylglyoxal, and biacetyl in bulk aqueous solutions that contain ammonium salts like ammonium sulfate (AS) (Grace et al., 2020; Kampf

50 et al., 2016; Nozière et al., 2009; Sareen et al., 2010; Yu et al., 2011), and to an extent from aerosol chamber studies (De Haan et al., 2017, 2018; Galloway et al., 2009, 2011). Bulk solutions can mimic the aqueous phase of actual atmospheric particles, albeit at lower ionic strength and reagent concentrations, higher water content, and without surface effects, which may influence particle phase chemistry of dicarbonyls (Yan et al., 2016; McNeill, 2015; Lee et al., 2013). The extrapolation of chemistry quantified in bulk solutions to atmospheric particles is evaluated in another study (Hensley et al., 2021, in prep).

55 Bulk solutions have the additional advantage that established organic analysis methods like nuclear magnetic resonance (NMR), mass spectrometry (MS), and UV/Vis spectroscopy can be used to identify reaction products and quantify reaction rates. The reaction mechanisms can inform chemical models that estimate for example the warming effect of brown carbon on climate (Ervens, 2015; Saleh, 2020).

      When glyoxal, methylglyoxal, or biacetyl and ammonium salts are introduced to an aqueous mixture, the medium

60 darkens. The color change has been attributed to accretion products that in spite of their low abundance can absorb light effectively (Grace et al., 2020; Kampf et al., 2012; Nozière et al., 2007; Shapiro et al., 2009; Yu et al., 2011). Irreversible reaction with NH$_X$ produces nitrogen-containing unsaturated rings, e.g., imidazoles in the glyoxal/NH$_X$ reaction, and is the starting point for further accretion reactions. Yu et al. (2011) and Kampf et al. (2012) demonstrate that imidazole formation

from glyoxal/NH$_X$ follows a rate law of the form k[GL]^2[NH$_4^+$][NH$_3$], and is as such fastest at neutral to basic pH (Maxut, 2015). Noziere et al. (2009) suggest that glyoxal/NH$_X$ is second order at low reactant concentrations, where imine formation is the rate-limiting step (Sedehi et al., 2013). Although imidazoles have also been detected in chamber experiments of deliquesced AS aerosol, the reaction is observed to be too slow at typical dicarbonyl concentrations and aerosol pH and NH$_X$

70   to affect chemical composition (Galloway et al., 2009; Yu et al., 2011). However, glyoxal/NH$_X$ reactions have been shown to be greatly accelerated in evaporating cloud droplets (Lee et al., 2013) and produce strongly absorbing compounds even at low concentrations (Shapiro et al., 2009). Methylglyoxal/NH$_X$ reactions in bulk solutions are faster and are shown to be linearly dependent on methylglyoxal and ammonium, but they too may be limited in the atmosphere (Powelson et al., 2014; Sareen et al., 2010; Sedehi et al., 2013). Biacetyl/NH$_X$ reactions are also shown to be linearly dependent on the dicarbonyl and

75   ammonium and can form light-absorbing species, although biacetyl is much less hydratable and is not as relevant to aqueous aerosol due to its much lower Henry's law constant (Grace et al., 2020). Further supported by field observations, modeling, and other laboratory work, the consensus is that dicarbonyl/NH$_X$ reactions probably are too slow to contribute substantial particle mass in the atmosphere (Ervens and Volkamer, 2010; Laskin et al., 2015).

        Beyond reaction with NH$_X$, past work with α-dicarbonyls suggests that the dicarbonyl family tends to behave
80   similarly in aqueous solutions. At basic pH, methylglyoxal and glyoxal both react with OH$^-$ to form colorless oligomeric products. Both are hydratable when dissolved in an aqueous solution, and therefore have suppressed vapor pressures over aqueous media. However, there are key differences in the behavior of these compounds, which have been attributed to the dicarbonyl moiety. Glyoxal favors a dihydrate state in dilute solutions that can oligomerize with mono- or unhydrated glyoxal to form cyclic hemiacetals. Methylglyoxal hydration occurs predominantly at the aldehyde, resulting in a ketodiol that is much

85   less reactive than glyoxal's monohydrate, which possesses an aldehydic group. Oligomerization of methylglyoxal and biacetyl proceeds predominantly through aldol condensation rather than through the formation of acetals. In the presence of anions like sulfate, methylglyoxal vapor pressure is increased (salting out) whereas glyoxal's decreases (salting in) (Kampf et al., 2013; Wang et al., 2014; Waxman et al., 2015; Galloway et al., 2009; Kroll et al., 2005). The accumulation of such dissimilarities can lead to different overall reactivities and solubilities between glyoxal and methylglyoxal. For example, glyoxal has an

90   effective Henry's Law constant that can be ~4 orders of magnitude larger than methylglyoxal when partitioning over salt-containing solutions (McNeill, 2015; Waxman et al., 2015), which can impact the loading and composition of atmospheric aerosol. The Henry's law constant of biacetyl is even lower than that of methylglyoxal. In general, it is thought that behavioral differences can be explained by the ketone versus aldehyde content of dicarbonyls and thus a dialdehyde is expected to behave more similarly to another dialdehyde, especially an electron poor one, than a ketoaldehyde or diketone.

95   The influence of carbon backbone structure on dicarbonyl reactivity has received far less attention, including in reactions with NH$_X$. Kampf et al. (2016) observed that the reactions of two larger dicarbonyls, 2,5-hexadione (an unsaturated 1,4-diketone) and glutaraldehyde (an unsaturated 1,5-dialdehyde), with NH$_X$ are fast, and their products may be more light-absorbing than those of α-dicarbonyls/NH$_X$ reactions. Building off of this work, we investigate butenedial reactions in aqueous

solutions containing NH_X and compare them to those of α-dicarbonyls. Butenedial is an unsaturated 1,4-dialdehyde known to be a major oxidation product of atmospherically abundant aromatics and furans (Bierbach et al., 1994; Coggon et al., 2019; Stockwell et al., 2015; Strollo and Ziemann, 2013; Volkamer et al., 2001; Raoult et al., 2004; Müller et al., 2016). Laboratory studies of OH oxidation of precursor compounds have recorded butenedial yields of 10.3% (Berndt and Böge, 2006) and 16% (Gómez Alvarez et al., 2007) from benzene; 13% (Gómez Alvarez et al., 2007) and 11-32% (Arey et al., 2009) from toluene; 10-29% (Arey et al., 2009) from *o*-xylene; and 99% (Gómez Alvarez et al., 2009) and 75% from furan (Aschmann et al., 2014). Butenedial and other dicarbonyls were detected in ambient air samples with elevated loading of aromatic hydrocarbons (Obermeyer et al., 2009). To the best of our knowledge, butenedial has not yet been quantitatively measured in field studies, in part due to the aforementioned challenges of measuring dicarbonyls. As butenedial is an electron-poor dialdehyde, its chemical reactivity is expected to be more similar to that of glyoxal than methylglyoxal or biacetyl. However, we have shown in a past study that butenedial acetal oligomers are insignificant in water and that it salts out in the presence of anions, behavior that is unlike that of glyoxal and more similar to methylglyoxal (Birdsall et al., 2019).

Butenedial is studied first in aqueous solutions without NH_X, in which it reacts reversibly with H_2O and irreversibly with OH^-. Then it is studied in AS aqueous solutions, in which it can additionally react irreversibly with NH_X. Reaction products and reaction rates are observed with NMR to characterize the chemical scheme and model kinetic mechanism. The reactivity of butenedial is compared to glyoxal as well as methylglyoxal and biacetyl. Implications for unsaturated 1,4- and other dicarbonyls are considered. The atmospheric relevance of dicarbonyl/NH_X reactions is re-examined, including as a source of brown carbon.

2 Methods

A chemical scheme and model kinetic mechanism was developed for butenedial in an aqueous NH_X solution. Butenedial reaction with OH^- or NH_X was studied in bulk solutions with conditions given in Table 1. As is shown later, reaction with OH^- was found to be negligible at the pH and NH_X conditions of the butenedial/NH_X reaction studies, and vice versa, indicating that butenedial/OH^- and butenedial/NH_X reactions were studied in isolation of one another. No other reactions were observed. Measurements of the composition of the bulk solutions were taken with NMR and MS and identified reaction products were used to formulate a chemical scheme. A custom model kinetic mechanism was fit to the temporal evolutions of reactants and reaction products (via NMR only), from which rate constants were empirically determined. Predictions with the model kinetic mechanism were compared against additional experimental measurements at different pH and NH_X.

2.1 Materials and instruments

All chemicals were obtained from Sigma Aldrich unless otherwise specified. The synthesis of butenedial is described elsewhere in greater detail (Avenati and Vogel, 1982; Birdsall et al., 2019). Mixtures containing 2.4 M 2,5-dihydro 2,5-dimethoxyfuran (TCI America, 98%) and 3.4 M glacial acetic acid (HAc, VWR, 99.7%) were prepared. After about 10 days

of reaction at room temperature, we purified mixtures with rotary evaporation to 75% butenedial by weight (w/w). An HSQC 13C-1H NMR of a ~0.5 M butenedial sample is provided in Figure S1. The remaining 25% was predominantly residual water and HAc. All mixtures were well mixed at the start of reactions. Reacting mixtures were kept in capped glass vials or capped NMR tubes without further stirring.

150   All 1D 1H-NMR spectra were collected with Varian 400 MHz spectrometers, 64 scans per recorded spectrum. Deuterium oxide (D_2O, 99.9 atom % D) was the solvent for NMR experiments. The methods described by Yu et al. (2011) were followed to estimate molarities quantitatively in 1H-NMR spectra with 1% w/w dimethyl sulfone (DMS, 99%). The pH was estimated from the spectra by tracking the proton shift of an acid near 50% dissociation, according to the methods described by Yu et al. (2011). The acid that was tracked depended on the solution pH: if solution pH 3-6, residual acetic acid

155 was tracked; if solution pH 6-8.5, 1% w/w methylphosphonic acid (MPA, 98%) was added and tracked; and if solution pH 9-11, 1% w/w 2,4,6-trimethylphenol (TMP, 99%) was added and tracked.

       MS spectra were collected of butenedial/OH^- mixtures with a liquid chromatography – mass spectrometry (LC-MS) and of butenedial/NH_X mixtures with both UV/Vis-LC-MS and a commercial time-of-flight mass spectrometer (TOF-MS, JEOL AccuTOF). Birdsall et al. (2018) describes the operation of the TOF-MS described in detail. ~140 pL aqueous particles

160 were produced from the analyte solution with a droplet-on-demand injector. The particles were briefly (< 1 s) in contact with dry nitrogen gas. Reaction and evaporation of solutes were negligible while the particles traveled from injector to a glass slide heated at 220 °C. The glass slide heated the particle, and a corona discharge ionized the resulting vapors to be drawn into the inlet of the TOF-MS. Mass spectral signals were recorded as counts per integer mass-to-charge (m/z) channel. 10-20% w/w hexaethylene glycol (PEG-6, 99%) was used as an internal standard for MS measurements, as done previously (Birdsall et al.,

165 2018). Previous work demonstrated there is no reaction between butenedial and PEG-6 (Birdsall et al., 2019). Distilled H_2O was the solvent for all MS experiments. Butenedial/NH_X experiments were measured with MS operated in positive mode while butenedial/OH^- experiments were taken with MS operated in negative mode, coupled with UV-Vis spectroscopy.

2.2 Chemical analysis

2.2.1 Butenedial in aqueous solutions without NH_X

170 0.55 M butenedial in D_2O solution and a six-fold dilution of this solution, resulting in 0.09 M butenedial in D_2O, were studied with NMR under acidic conditions. In both solutions, butenedial strongly favored the dihydrate form with only minimal formation of acetal oligomers (see Supplement Section 2, Figure S2 and Table S2), as shown previously (Birdsall et al., 2019). Additionally, four solutions containing 0.2-0.3 M butenedial were prepared in D_2O buffered with 1 M Na_2CO_3-$NaHCO_3$ to pH 8.8-10.4. All solutions immediately turned dark brown (Figure S16). Butenedial loss was measured quantitatively with NMR

175 throughout its reaction with OH^- (Figure S7). Analogous to, e.g., lactic acid or glycolic acid formation from methylglyoxal or glyoxal reaction with OH^-, respectively, we propose that butenedial disproportionates to hydroxycrotonic acid (Figure S4). Hydroxycrotonic acid was observed with LC-MS (Figure S5) and was found to absorb light between 300-450 nm (Figure S6).

185 The detection of hydroxycrotonic acid oligomers (Figure S5-S6) and the growth of broad peaks embedded in the baseline of 1H-NMR spectra (Figure S7) were indicative of accretion reactions.

2.2.2 Butenedial in aqueous solutions with NH_X

0.9 M butenedial/0.45 M AS (VWR, > 99%) mixtures were prepared in water and D_2O with the internal standards PEG-6 or
DMS and 0.5 M sodium carbonate (Na_2CO_3) – sodium bicarbonate ($NaHCO_3$) buffer. The solution immediately turned orange
190 brown (Figure S16). After 20 min of reaction, mass spectra of the mixtures indicated nitrogen-containing products with signals
at m/z 84, 149, 150, and 168, assumed to be adducts with H^+ (Figure S11). The most reasonable chemical formulas of these
products were C_4H_5NO (83 Da), $C_8H_8N_2O$ (148 Da), $C_8H_7NO_2$ (149 Da), and $C_8H_9NO_3$ (167 Da). $C_8H_9NO_3$ was the parent
molecule for the $C_8H_7NO_2$ fragment. C_4H_5NO (83 Da), $C_8H_9NO_3$ (167 Da), and $C_8H_9NO_3$ (251 Da) were observed
unambiguously with high-resolution LC-MS measurement of an equivalent solution (Figure S12).

195 The 1H-NMR spectra (Figure S8) showed two distinct groups of quantitative related signals that had similar temporal
behavior (Table S5). Each group of peaks whose quantitative signal strength behaved as integers and had the same temporal
behavior was presumed to arise from a single compound. One group was assigned to C_4H_5NO and the other to $C_8H_9NO_3$
according to agreement in chemical evolution between MS and NMR measurements (Figure S15). A molecular structure was
proposed for each cluster of peaks and the molecular formulas mentioned above, according to NMR peak assignments and
200 analogous reactions (see SI Section 2.4, including Figures S9-S10). The inferred products were as follows: 2-pyrrolinone
(pyrrolinone, PR, C_4H_5NO), and a butenedial-pyrrolinone "dimer" (BD-PR, $C_8H_9NO_3$). We propose that 2-butenal-1,3-
diazepine (diazepine, DZ, $C_8H_8N_2O$) is a minor product that is observable with MS but was not detected with the less sensitive
NMR. The growth of broad peaks embedded in the baseline suggested substantial formation of accretion products (Figure
S14). Additionally, high-resolution LC-MS-UV/Vis measurements suggested evidence of pyrrolinone, butenedial-pyrrolinone
205 "dimer," and a "trimer" consisting of three butenedial and two NH_X (Figures S12-S13). In particular, the proposed "dimer"
and "trimer" are strongly π-conjugated and light-absorbing (Figures S12-S13). As such, accretion products composed of
butenedial, NHx, and pyrrolinone could explain the dark color of the solution (Figure S17).

2.3 Model kinetic mechanism

The model kinetic mechanism was formulated as a system of ordinary differential equations, one ordinary differential equation
210 per identified chemical compound. The butenedial reaction with OH^- was quantified and used as foundation for the mechanism
with NH_X. Rate laws were formulated based on known reactions of related species and then adjusted to optimize agreement
between the mechanism and observations (see Section 3). Python's scipy package was used to parameterize each fit rate
constant's mean value and standard error. The lmfit library with the Levenberg-Marquardt algorithm was used to perform the
least squares minimization. A Monte Carlo simulation was performed to derive the reported 95% confidence intervals on
215 model runs.

2.3.1 Butenedial/OH⁻ reaction

Dicarbonyl/OH⁻ reactions are known to be effectively irreversible and are characterized by a rate law that is first order in the dicarbonyl (R1). According to Fratzke & Reilly (1986), the dicarbonyl/OH⁻ reaction rate constant (k_1) is a function of OH⁻ as defined by the following relationship:

$$k_1 = \frac{a_{II}[OH^-] + a_{II}[OH^-]^2}{1 + a_{III}[OH^-]},$$ (1)

where a_I and a_{II} are related to the role of the hydrated anion or dianion, respectively (Fratzke and Reilly, 1986). The coefficients a_I, a_{II}, and a_{III} were fit with four unique [OH⁻]/k_1 pairings, each corresponding to a different experimental run. k_1 was derived from the first order loss of butenedial in each experiment (Figure S18). Subsequently, a_I-a_{III} were determined using the scipy optimize.curve_fit library implemented with the Trust Region Reflective minimization method.

2.3.2 Butenedial/NH$_X$ reaction

A system of three ordinary differential equations (DE1-DE3) was used to model butenedial, pyrrolinone, and butenedial-pyrrolinone dimer concentrations, with pH and initial concentrations of reactants and products as inputs. Rate constants for five rate laws (R2-R6) were fit to experimental data, with starting conditions of 0.9 M butenedial and 0.9 M NH$_X$, and pH ranging 4.2-5.7. k_1 was implemented according to the fitting described in Section 2.3.1. pH was affected by residual acetic acid from butenedial synthesis, ammonium sulfate, addition of carbonate buffer, and production of acid during reaction. pH was estimated with an empirical formulation that agreed closely with measurements (Figure S19). Model performance was assessed against measurements taken in bulk liquid experiments with different initial conditions and pH (Figures S21-S22). One limitation was that reaction rates of unmeasured species had to be approximated with a proxy, i.e., in the cases of NH$_X$ and accretion product concentrations. As is discussed in Section 3, the approximations have minimal impact on the prediction of butenedial loss and on the estimation of most parameters.

3 Results

A chemical scheme for butenedial in an aqueous solution with NH$_X$ is proposed in Section 3.1. Butenedial reaction with OH⁻ and reaction with NH$_X$ are described in Section 3.2 and Section 3.3, respectively. The fate of butenedial in aqueous solutions with and without NH$_X$ is summarized in Section 3.4.

3.1 Chemical scheme

Butenedial in aqueous NH$_X$ solutions of pH 3.6-10.4 is proposed to obey the chemical scheme shown in Figure 1, which demonstrates that it can undergo three reactions. First, butenedial can be reversibly hydrated and is observed to prefer the dihydrate form in aqueous solutions without evidence for significant acetal oligomer formation. Second, butenedial reacts with

OH⁻ to form irreversible reaction products such as a hydroxy acid, which ultimately lead to oligomeric, light-absorbing
compounds. Third, butenedial reacts with NH_3 to produce an imine intermediate which forms irreversible reaction products
(pyrrolinone, a diazepine, and a butenedial-pyrrolinone "dimer") and also ultimately lead to oligomeric, light-absorbing
compounds (Figure 12). These accretion products are observed to be reactive with reactants and products.

As discussed in a previous study, like glyoxal, the hydration equilibrium of butenedial is strongly shifted toward the
dihydrate (>95% of the total butenedial on a molar basis). Birdsall et al. (2019) also showed that the ratio of unhydrated or
monohydrated to dihydrated butenedial appeared to be unaffected by the availability of water. It is expected that the hydration
behavior of butenedial will affect its reactivity, and possibly differentiate it from glyoxal, which has been observed to form a
highly reactive yet soluble monohydrate form. Additionally, in contrast to glyoxal, which readily forms glyoxal acetal
oligomers, no butenedial acetal oligomers were observed by Birdsall et al. (2019). Our experiments support that only minimal
acetal oligomer formation is possible and is much less pronounced than for glyoxal. This behavior is not typical for dialdehydes
but has been observed for adipaldehyde (Hardy et al., 1972). One explanation is that butenedial, like adipaldehyde, has a
hydrophobic center that influences the ability of its hydrates to oligomerize like glyoxal.

The 1H-NMR spectra of butenedial in basic aqueous solutions and solutions with NH_X both exhibit the buildup of
signal in the baseline in the vicinity of possible monomer peaks (shifted to lower ppm, Figures S7, S14). This buildup increases
in intensity and spreads out with respect to chemical shift over time. Additionally, high-resolution LC-MS measurements
indicate substantial formation of accretion products through butenedial/NH_X and butenedial/OH⁻ reactions (Figures S5, S12).
Thus, accretion reactions take place that are the ultimate sink for butenedial and its reaction products, producing low-volatility
compounds that are light absorbing and can explain the brown color of reaction mixtures (Figures S6, S13). Reaction products
of dicarbonyl/OH⁻ reactions are not thought to be reactive to the dicarbonyl or to products of dicarbonyl/NH_X reactions, such
as in the case of glyoxal (Yu et al., 2011). Butenedial loss is observed to be first order in butenedial at all time scales and [OH⁻
], indicating that butenedial/OH⁻ reaction does not result in additional butenedial removal from solution, e.g., via products
reacting with butenedial. On the other hand, butenedial is reactive with butenedial/NH_X reaction products, as has been observed
in analogous reactions of glyoxal, methylglyoxal, and biacetyl, and they and higher accretion products increase butenedial
loss.

3.2 Butenedial/OH⁻ reaction

Estimates of the a-coefficients of k_1 are shown in Table 2. The dependence of the pseudo first-order rate constant k_1 on OH⁻ is
shown in Figure 2. The rate constant is $< 1 \times 10^{-4}$ s⁻¹ at pH < 9, indicating that butenedial/OH⁻ reaction is insignificant except at
basic pH. No evidence of reaction has been observed in standard butenedial solutions (pH ~ 4) that we have kept on the shelf
for months. At solution pH 8.5-8.8, butenedial loss from butenedial/OH⁻ reaction is negligible compared to butenedial/NH_X
reaction (Figure S21). We therefore conclude that butenedial/OH⁻ reaction is insignificant at neutral and acidic conditions
relevant to the atmosphere, especially when NH_X is present, although the parametrization is included in the butenedial/NH_X
model kinetic mechanism.

3.3 Butenedial/NH$_X$ reaction

Five chemical reactions (R2-R6) explain the evolution of butenedial (BD) and its major reaction products with NH$_X$, pyrrolinone (PR) and butenedial-pyrrolinone "dimer" (BD-PR). Table 3 shows the proposed reactions, their rate laws and fitted rate constants. The reactions and their rate laws are discussed here and the fitted rate constants in Section 3.3.2.

The initial, irreversible reaction between butenedial and NH$_3$ (R2) is linearly dependent on both species and produces pyrrolinone. While the reaction is acid catalyzed, the rate constant of dialdehyde/NH$_X$ reactions is pH dependent (Yu et al., 2011), resulting in a pH-independent rate law. At constant NH$_3$, the reaction is pseudo first order in butenedial. In analogy to the related glyoxal and methylglyoxal reactions, we propose an imine intermediate for this reaction. Reaction of pyrrolinone with butenedial is pH-dependent and produces a butenedial-pyrrolinone dimer (R3). We anticipate that the proposed imine can also undergo an acid-catalyzed reaction to produce a diazepine (DZ).

Reactions between each of butenedial, pyrrolinone, butenedial-pyrrolinone dimer and an accretion product term (R4-R6) are included to represent the removal of these species through accretion reactions. Accretion reactions have been observed in studies with glyoxal (Kampf et al., 2012; Yu et al., 2011). These reactions typically involve oligomer-like molecules made up of precursor compounds (in this case, butenedial), its reaction products (pyrrolinone and butenedial-pyrrolinone dimer), and products of subsequent reactions (e.g., the proposed pyrrolinone-butenedial-pyrrolinone "trimer," Figure S12). The resulting accretion products are diverse, as is known for similar chemical systems, and were not quantified directly with 1H-NMR. Therefore, to include these reactions in the model kinetic mechanism, the accretion product (AP) concentration is approximated with butenedial-pyrrolinone dimer as a proxy: [AP] = [BD-PR]. Setting the AP concentration equal to BD-PR concentration involves several assumptions, namely that the number of AP reactive sites scales with BD-PR concentration, the molecular weight distribution of AP members is independent of pH, and any reversibility in accretion reactions can be accounted for with this approximation. However, strong agreement is still observed between butenedial observations and model predictions under different pH and initial reactant conditions, which suggests that this approximation does not significantly affect mechanistic portrayal of butenedial reactivity.

$$\frac{d[BD]}{dt} = -k_1[BD] - k_2[BD][NH_3] - k_3[BD][PR][OH^-] - k_4[BD][AP] \qquad \text{(DE1)}$$

$$\frac{d[PR]}{dt} = k_2[BD][NH_3] - k_3[BD][PR][OH^-] - k_5[PR][AP] \qquad \text{(DE2)}$$

$$\frac{d[BD\text{-}PR]}{dt} = k_3[BD][PR][OH^-] - k_6[BD\text{-}PR][AP] \qquad \text{(DE3)}$$

325

The butenedial/NH$_X$ model kinetic mechanism contains three differential equations (DE1-DE3), one per explicitly measured species: butenedial (BD), pyrrolinone (PR), and butenedial-pyrrolinone dimer (BD-PR). The finalized mechanism contains the best fit reaction rate constants to experimental data; the resulting model output and experimental data are shown

in Figure 3. The mechanism correctly captures the evolution of each species across the wide range of pH and reactant
330 concentrations in the experiment, which are especially relevant to those typical of atmospheric particles.

pH is modeled independently with an empirically derived fit. The fitting of pH to the empirical law causes a maximum deviation of 0.1 pH units from measured pH (Figure S19). For the fitting, NH_X is not measured and instead is estimated with the following relationship: $[NH_X] = [NH_{X,0}] - ([BD_0] - [BD])$, i.e., one NH_X is lost per butenedial. This simplification artificially consumes NH_X when butenedial dimerizes with pyrrolinone or accretes, and NH_X loss could be overestimated. To
335 assess the sensitivity of the parametrization to NH_X, the model fitting was also performed assuming NH_X is not consumed during reaction (i.e., zero NH_X is lost per burtenedial). The parameter fitting with this scenario provides a maximum deviation as it is effectively the opposite extreme. The differences between these produced parameters and those of the original fitting were small, typically falling <5% of the parameter estimates with one exception (Figure S20). The employed simplification of NH_X is therefore assumed to have minor effects on the model kinetic mechanism.

340 Model predictions using this mechanism compare well with measurements from two additional experiments with different pH and initial conditions (Figure S21-S22). One was performed with 0.4 M BD_0, 0.4 M $NH_{X,0}$, and pH 3.6 and the other with 0.9 M BD_0, 0.2 M $NH_{X,0}$, and pH 8.5-8.8. This indicates that the model kinetic mechanism is robust across a relevant range of pH and initial conditions.

3.4 Comparison of butenedial loss processes in aqueous aerosols

345 The lifetime of condensed-phase butenedial from aqueous reaction with OH^- or NH_X, with AS as NH_X source, is compared to that of wet deposition, which for tropospheric aqueous particles is about one week (Seinfeld and Pandis, 2016). The dominant first order loss process of butenedial is shown as a function of NH_X and pH in Figure 4. Butenedial/OH^- is the main sink if < 1 mM NH_X and above ~pH 7, although this pH is not particularly atmospherically relevant. Reaction with NH_X can be fast at typical NH_X, even under somewhat acidic conditions, and is therefore competitive with wet deposition. Butenedial loss is
350 increased through accretion reactions in the NH_X pathway but this effect is not included in this analysis. Thus, the figure represents a lower limit for butenedial loss via the NH_X pathway.

4 Discussion

4.1 Comparison of dicarbonyl reactivity in aqueous NH_X solutions

The reactivity of dicarbonyls in aqueous NH_X solutions was previously understood primarily on the basis of the dominant
355 functionality through studies of α-dicarbonyls. Following the work of Kampf et al. (2016), this study provides an additional perspective that considers the role of the carbon skeleton on dicarbonyl behavior. Biacetyl is the least hydratable of the α-dicarbonyls, and because it is a diketone, is the least similar to butenedial. Methylglyoxal is less hydrated than glyoxal and butenedial because it is a ketoaldehyde that has a hydrophobic methyl moiety. Butenedial is an electron-poor dialdehyde like

glyoxal and is therefore strongly hydrated, but it also has a hydrophobic alkene group. In addition, it has a four-carbon chain, making the formation of stable five-membered organic molecules thermodynamically and especially kinetically favorable in
365 comparison to glyoxal, methylglyoxal, and biacetyl, which provides evidence for the importance of the carbon backbone to dicarbonyl chemistry.

The dicarbonyl moiety leads to several similarities in the behavior of butenedial, glyoxal, methylglyoxal, and, to a lesser degree, biacetyl in aqueous NH_X solutions: all hydrate reversibly, react with OH^- under basic conditions, and react with NH_X to produce heterocycles and subsequently undergo accretion reactions. Brown carbon is produced in solution even if
370 minimal reaction has occurred and accelerates with increasing pH. However, we demonstrate three important differences between butenedial and glyoxal in particular that showcase the variability possible between dicarbonyls and even electron-poor dialdehydes.

First, unlike butenedial, glyoxal shows a strong tendency to form acetal oligomers in pure aqueous solutions. Biacetyl and methylglyoxal can also form acetal oligomers in aqueous solutions, although aldol condensation products are more
375 common (Grace et al., 2020; Sareen et al., 2010). Somewhat surprisingly, butenedial acetal oligomers are much less pronounced, despite butenedial having two reactive aldehyde groups and being predominantly dihydrated in aqueous solution. This behavior was reported by Birdsall et al. (2019) who did not find any acetal products from butenedial itself or, perhaps even more surprisingly, in the presence of high concentrations of polyethylene glycol. One explanation could be that butenedial, like methylglyoxal and biacetyl, has a substantial hydrophobic component that influences the ability of its hydrates
380 to oligomerize like glyoxal, which was not expected based on the similarity with glyoxal in hydration behavior.

It is also observed that the double bond within the carbon backbone affects the properties of the products. Polymers of lactic acid and glycolic acid (the products of methylglyoxal and glyoxal reaction with OH^-) are colorless, presumably because they lack π-conjugated double bonds. Oligomers of hydroxycrotonic acid from butenedial/OH^- reaction on the other hand efficiently absorb light even at relatively low quantities (browning was observed immediately after introducing butenedial
385 to basic conditions). The light absorptivity of the products can be attributed to the alkene bond they inherit from butenedial and potentially the presence of carbonyls. Therefore, it is suggested that other unsaturated dicarbonyls could lead to the production of light-absorbing compounds, although unsaturated compounds and basic pH are not expected to be relevant in atmospheric aerosols.

The third important difference is the rate and rate law for the dominant products of the dicarbonyl/NH_X reactions. We
390 do not suggest that NH_4^+ is a catalyst (as a source of Bronsted acid) for butenedial/NH_3 reaction, which has been proposed by previous studies for glyoxal (Nozière et al., 2009). While imidazole production is second order in glyoxal and NH_3 and explicitly pH dependent (Yu et al., 2011), pyrrolinone production is linearly dependent on butenedial and NH_3, which is similar to methylglyoxal (Sareen et al., 2010) and biacetyl (Grace et al., 2020). This may not be surprising because in contrast to the two-carbon glyoxal, reaction between one butenedial and one NH_3 already results in a stable heterocycle. We suggest that
395 dicarbonyls with at least two carbons between carbonyl groups can form heterocycles with bimolecular rate laws. They could include four-carbon dicarbonyls (e.g., succinaldehyde, 4-oxopentanal, other unsaturated or saturated 1,4-dicarbonyls) and

phthalaldehyde, which can form five-membered rings, and five-carbon dicarbonyls (e.g., glutaraldehyde) that are capable of forming pyridines and other six-membered heterocycles, as shown by Kampf et al. (2016). Electron poor dialdehydes with longer carbon backbones (six-carbon or more) may also be able to produce stable products from self reactions. Notably,

405 butenedial reaction with NH_3 is much faster than for glyoxal, methylglyoxal, and biacetyl. Yu et al. (2011) showed that only 12% of the initial glyoxal in a 1 M glyoxal/1 M AS solution had been consumed over 5.5 months, whereas at comparable pH we observed 11% removal of butenedial in a 0.4 M butenedial/0.2 M AS solution after 8 hours. Similarly, the lifetime of methylglyoxal with respect to reaction with NH_4^+ in a 14 M AS solution is 29.8 hours (Sareen et al., 2010), however we calculate a corresponding lifetime of 4.2 hours at pH 4, and 2.5 minutes at pH 6 for butenedial. The fast rate of butenedial/NH_X

410 reaction supports other work that has shown more rapid brown carbon formation from larger dicarbonyls than for α-dicarbonyls (Kampf et al., 2016).

In sum, this work complements a previous study (Birdsall et al., 2019) to show that it is difficult to extrapolate the physicochemical properties of reactive dicarbonyls from their α-dicarbonyl prototypes. Not only the reactive functional groups affect reactivity but the structure of the carbon backbone as well. In the case of glyoxal, it is likely that its vicinal two aldehydes

415 cause its chemical and physical properties to be unique and dissimilar to the rest of the dialdehydes/dicarbonyls. Further studies should be conducted with other more complex dicarbonyls to elucidate patterns in chemical behavior that are related to the carbon skeleton.

4.2 Atmospheric implications

This work shows that the aqueous reaction of butenedial with and without NH_X can form low-volatility chromophores that will

420 be retained in the condensed phase and absorb radiation. The results, especially the rapid reaction of butenedial with NH_X, show that similarly reactive dicarbonyls could impact chemical composition and optical properties of particles, and thus directly influence the human health and climate impacts of particles.

Butenedial was recently shown to have a gas-phase photochemical lifetime of 10-15 minutes due to photolysis (Newland et al., 2019) although its high effective Henry's Law constant (6x10^7 M atm^{-1}, Birdsall et al., 2019) can allow

425 effective partitioning into the aqueous phase. Butenedial/OH$^-$ reactions are too slow at typical atmospheric pH values to contribute significantly. It is, however, likely that condensed phase reaction of butenedial with NH_X could regionally be important, specifically at close to neutral pH and high NH_X, such as in agricultural areas in India or the North China Plain where NH_3 emissions are high (Kuttippurath et al., 2020; Zhang et al., 2010) and aerosol may be alkaline (Kulshrestha et al., 2001; Tao et al., 2020). For example, recent work suggests that near-surface particle pH is 4.4-5.7 in the NCP and in some

430 locations, could be consistently > 6 (Tao et al., 2020). At pH 6 and 4 M NH_X, the lifetime of butenedial against reaction with NH_X is only 18 minutes, even excluding enhancements from reaction with pyrrolinone and other accretion reactions or, in the atmosphere, other reactive organics. The results show that accretion reactions, and therefore the accumulation of chromophores, increase strongly with pH. Dimers and accretion products correspond to the vast majority of products (and

quickly pull more butenedial out of solution) at slightly acidic or neutral pH. An important future research step is to refine the relationship between pH and oligomerization/accretion reaction rates.

We do not propose that butenedial alone contributes significant brown carbon. However, the reactivity of butenedial can be extrapolated to dicarbonyls for which condensed phase chemistry has not been studied. Such dicarbonyls are rarely measured but could be abundant. For example, 4-oxopentanal (a saturated 1,4-ketoaldehyde) was recorded at particulate concentrations averaging 62.7 ng m^{-3} over a Japanese forest (Matsunaga et al., 2004); for a typical aerosol liquid water content of 1-10 mg m^{-3}, this corresponds to particulate 4-oxopentanal concentrations of approximately 6-60 mM, which was similar to that of glyoxal and methylglyoxal. If 4-oxopentanal is representative of a range of dicarbonyls that react with NH$_X$ like butenedial, then the reaction could be fast enough that the sum of dicarbonyls may constitute a regional source of brown carbon in regions with high NH$_X$ and alkalinity. The vast majority of studies of the condensed-phase atmospheric chemistry of dicarbonyls have focused on glyoxal, methylglyoxal, and biacetyl, in part because they are abundant and commercially available. The fact that butenedial has much faster reaction rates of forming brown carbon that are first order with respect to the dicarbonyl indicates that additional studies of larger dicarbonyls with hydrophobic moieties are needed, especially to further evaluate the role of dicarbonyls in the formation of brown carbon.

Code and data availability. The Python package pyrosolchem used as the kinetic model of droplet evaporation is available at https://github.com/jackattack1415/pyrosolchem (last access: 23 February 2021). Data used to generate paper figures are available upon request.

Author contributions. JCH, AWB, and FNK designed the experiments. AWB, JCH, and GV performed the butenedial synthesis. JCH and JLC performed the NMR experiments. JCH performed the MS experiments. JCH analyzed the data and produced the model characterization. JCH prepared the paper with contributions from all co-authors.

Competing interests. The authors declare that they have no conflict of interest.

Financial support. This research has been supported by the National Science Foundation, Division of Chemistry (grant no. 1808084) and the Harvard University Faculty of Arts and Sciences Dean's Competitive Fund for Promising Scholarship.

References

Andreae, M. O. and Gelencser, A.: Black carbon or brown carbon? The nature of light-absorbing carbonaceous aerosols, 18, 2006.

Arey, J., Obermeyer, G., Aschmann, S. M., Chattopadhyay, S., Cusick, R. D., and Atkinson, R.: Dicarbonyl Products of the OH Radical-Initiated Reaction of a Series of Aromatic Hydrocarbons, Environ. Sci. Technol., 43, 683–689, https://doi.org/10.1021/es8019098, 2009.

Aschmann, S. M., Nishino, N., Arey, J., and Atkinson, R.: Kinetics of the Reactions of OH Radicals with 2- and 3-Methylfuran, 2,3- and 2,5-Dimethylfuran, and *E* - and *Z* -3-Hexene-2,5-dione, and Products of OH + 2,5-Dimethylfuran, Environ. Sci. Technol., 45, 1859–1865, https://doi.org/10.1021/es103207k, 2011.

Aschmann, S. M., Nishino, N., Arey, J., and Atkinson, R.: Products of the OH Radical-Initiated Reactions of Furan, 2- and 3-Methylfuran, and 2,3- and 2,5-Dimethylfuran in the Presence of NO, J. Phys. Chem. A, 118, 457–466, https://doi.org/10.1021/jp410345k, 2014.

Avenati, M. and Vogel, P.: Face Selectivity of theDiels-Alder Additions of 2-Substituted 5,6-bis((E)-chloromethylidene)bicyclo[2.2.2]octanes, Helv. Chim. Acta, 65, 204–216, https://doi.org/10.1002/hlca.19820650119, 1982.

Berndt, T. and Böge, O.: Formation of phenol and carbonyls from the atmospheric reaction of OH radicals with benzene, Phys. Chem. Chem. Phys., 8, 1205, https://doi.org/10.1039/b514148f, 2006.

Bierbach, Arwid., Barnes, Ian., Becker, K. H., and Wiesen, Evelyn.: Atmospheric Chemistry of Unsaturated Carbonyls: Butenedial, 4-Oxo-2-pentenal, 3-Hexene-2,5-dione, Maleic Anhydride, 3H-Furan-2-one, and 5-Methyl-3H-furan-2-one, Environ. Sci. Technol., 28, 715–729, https://doi.org/10.1021/es00053a028, 1994.

Birdsall, A. W., Krieger, U. K., and Keutsch, F. N.: Electrodynamic balance–mass spectrometry of single particles as a new platform for atmospheric chemistry research, Atmos. Meas. Tech., 11, 33–47, https://doi.org/10.5194/amt-11-33-2018, 2018.

Birdsall, A. W., Hensley, J. C., Kotowitz, P. S., Huisman, A. J., and Keutsch, F. N.: Single-particle experiments measuring humidity and inorganic salt effects on gas-particle partitioning of butenedial, Atmos. Chem. Phys., 19, 14195–14209, https://doi.org/10.5194/acp-19-14195-2019, 2019.

Bond, T. C., Bhardwaj, E., Dong, R., Jogani, R., Jung, S., Roden, C., Streets, D. G., and Trautmann, N. M.: Historical emissions of black and organic carbon aerosol from energy-related combustion, 1850-2000: HISTORICAL BC/OC EMISSIONS, Global Biogeochem. Cycles, 21, n/a-n/a, https://doi.org/10.1029/2006GB002840, 2007.

Coggon, M. M., Lim, C. Y., Koss, A. R., Sekimoto, K., Yuan, B., Gilman, J. B., Hagan, D. H., Selimovic, V., Zarzana, K. J., Brown, S. S., Roberts, J. M., Müller, M., Yokelson, R., Wisthaler, A., Krechmer, J. E., Jimenez, J. L., Cappa, C., Kroll, J. H., de Gouw, J., and Warneke, C.: OH chemistry of non-methane organic gases (NMOGs) emitted from laboratory and ambient biomass burning smoke: evaluating the influence of furans and oxygenated aromatics on ozone and secondary NMOG formation, Atmos. Chem. Phys., 19, 14875–14899, https://doi.org/10.5194/acp-19-14875-2019, 2019.

De Haan, D. O., Hawkins, L. N., Welsh, H. G., Pednekar, R., Casar, J. R., Pennington, E. A., de Loera, A., Jimenez, N. G., Symons, M. A., Zauscher, M., Pajunoja, A., Caponi, L., Cazaunau, M., Formenti, P., Gratien, A., Pangui, E., and Doussin, J.-F.: Brown Carbon Production in Ammonium- or Amine-Containing Aerosol Particles by Reactive Uptake of Methylglyoxal and Photolytic Cloud Cycling, Environ. Sci. Technol., 51, 7458–7466, https://doi.org/10.1021/acs.est.7b00159, 2017.

De Haan, D. O., Jimenez, N. G., de Loera, A., Cazaunau, M., Gratien, A., Pangui, E., and Doussin, J.-F.: Methylglyoxal Uptake Coefficients on Aqueous Aerosol Surfaces, J. Phys. Chem. A, 122, 4854–4860, https://doi.org/10.1021/acs.jpca.8b00533, 2018.

Debus, H.: Ueber die Einwirkung des Ammoniaks auf Glyoxal, 107, 199–208, https://doi.org/10.1002/jlac.18581070209, 1858.

Ervens, B.: Modeling the Processing of Aerosol and Trace Gases in Clouds and Fogs, Chem. Rev., 115, 4157–4198, https://doi.org/10.1021/cr5005887, 2015.

Ervens, B. and Volkamer, R.: Glyoxal processing by aerosol multiphase chemistry: towards a kinetic modeling framework of secondary organic aerosol formation in aqueous particles, Atmos. Chem. Phys., 10, 8219–8244, https://doi.org/10.5194/acp-10-8219-2010, 2010.

Fratzke, A. R. and Reilly, P. J.: Kinetic analysis of the disproportionation of aqueous glyoxal, Int. J. Chem. Kinet., 18, 757–773, https://doi.org/10.1002/kin.550180704, 1986.

Galloway, M. M., Chhabra, P. S., Chan, A. W. H., Surratt, J. D., Flagan, R. C., Seinfeld, J. H., and Keutsch, F. N.: Glyoxal uptake on ammonium sulphate seed aerosol: reaction products and reversibility of uptake under dark and irradiated conditions, 15, 2009.

Galloway, M. M., Loza, C. L., Chhabra, P. S., Chan, A. W. H., Yee, L. D., Seinfeld, J. H., and Keutsch, F. N.: Analysis of photochemical and dark glyoxal uptake: Implications for SOA formation: PHOTOCHEMICAL AND DARK GLYOXAL UPTAKE, Geophys. Res. Lett., 38, n/a-n/a, https://doi.org/10.1029/2011GL048514, 2011.

Gómez Alvarez, E., Viidanoja, J., Muñoz, A., Wirtz, K., and Hjorth, J.: Experimental Confirmation of the Dicarbonyl Route in the Photo-oxidation of Toluene and Benzene, Environ. Sci. Technol., 41, 8362–8369, https://doi.org/10.1021/es0713274, 2007.

Gómez Alvarez, E., Borrás, E., Viidanoja, J., and Hjorth, J.: Unsaturated dicarbonyl products from the OH-initiated photo-oxidation of furan, 2-methylfuran and 3-methylfuran, Atmospheric Environment, 43, 1603–1612, https://doi.org/10.1016/j.atmosenv.2008.12.019, 2009.

Grace, D. N., Lugos, E. N., Ma, S., Griffith, D. R., Hendrickson, H. P., Woo, J. L., and Galloway, M. M.: Brown Carbon Formation Potential of the Biacetyl–Ammonium Sulfate Reaction System, ACS Earth Space Chem., 4, 1104–1113, https://doi.org/10.1021/acsearthspacechem.0c00096, 2020.

Hamilton, J. F., Lewis, A. C., Bloss, C., Wagner, V., Henderson, A. P., Golding, B. T., Wirtz, K., Martin-Reviejo, M., and Pilling, M. J.: Measurements of photo-oxidation products from the reaction of a series of alkyl-benzenes with hydroxyl radicals during EXACT using comprehensive gas chromatography, 16, 2003.

Hardy, P. M., Nicholls, A. C., and Rydon, H. N.: The hydration and polymerisation of succinaldehyde, glutaraldehyde, and adipaldehyde, 2270, https://doi.org/10.1039/p29720002270, 1972.

Kampf, C. J., Jakob, R., and Hoffmann, T.: Identification and characterization of aging products in the glyoxal/ammonium sulfate system – implications for light-absorbing material in atmospheric aerosols, Atmos. Chem. Phys., 12, 6323–6333, https://doi.org/10.5194/acp-12-6323-2012, 2012.

Kampf, C. J., Waxman, E. M., Slowik, J. G., Dommen, J., Pfaffenberger, L., Praplan, A. P., Prévôt, A. S. H., Baltensperger, U., Hoffmann, T., and Volkamer, R.: Effective Henry's Law Partitioning and the Salting Constant of Glyoxal in Aerosols Containing Sulfate, Environ. Sci. Technol., 47, 4236–4244, https://doi.org/10.1021/es400083d, 2013.

Kampf, C. J., Filippi, A., Zuth, C., Hoffmann, T., and Opatz, T.: Secondary brown carbon formation via the dicarbonyl imine pathway: nitrogen heterocycle formation and synergistic effects, Phys. Chem. Chem. Phys., 18, 18353–18364, https://doi.org/10.1039/C6CP03029G, 2016.

Kanakidou, M., Seinfeld, J. H., Pandis, S. N., Barnes, I., Dentener, F. J., Facchini, M. C., Dingenen, R. V., Ervens, B., Nenes, A., Nielsen, C. J., Swietlicki, E., Putaud, J. P., Balkanski, Y., Fuzzi, S., Horth, J., Moortgat, G. K., Winterhalter, R., Myhre, C. E. L., Tsigaridis, K., Vignati, E., Stephanou, E. G., and Wilson, J.: Organic aerosol and global climate modelling: a review, 71, 2005.

Kroll, J. H., Ng, N. L., Murphy, S. M., Varutbangkul, V., Flagan, R. C., and Seinfeld, J. H.: Chamber studies of secondary organic aerosol growth by reactive uptake of simple carbonyl compounds, J. Geophys. Res., 110, D23207, https://doi.org/10.1029/2005JD006004, 2005.

Kulshrestha, U. C., Kulshrestha, M. J., Sekar, R., Vairamani, M., Sarkar, A. K., and Parashar, D. C.: Investigation of Alkaline Nature of Rain Water in India, Water, Air, & Soil Pollution, 130, 1685–1690, https://doi.org/10.1023/A:1013937906261, 2001.

Kuttippurath, J., Singh, A., Dash, S. P., Mallick, N., Clerbaux, C., Van Damme, M., Clarisse, L., Coheur, P.-F., Raj, S., Abbhishek, K., and Varikoden, H.: Record high levels of atmospheric ammonia over India: Spatial and temporal analyses, Science of The Total Environment, 740, 139986, https://doi.org/10.1016/j.scitotenv.2020.139986, 2020.

Laskin, A., Laskin, J., and Nizkorodov, S. A.: Chemistry of Atmospheric Brown Carbon, Chem. Rev., 115, 4335–4382, https://doi.org/10.1021/cr5006167, 2015.

Lee, A. K. Y., Zhao, R., Li, R., Liggio, J., Li, S.-M., and Abbatt, Jonathan. P. D.: Formation of Light Absorbing Organo-Nitrogen Species from Evaporation of Droplets Containing Glyoxal and Ammonium Sulfate, Environ. Sci. Technol., 47, 12819–12826, https://doi.org/10.1021/es402687w, 2013.

Loeffler, K. W., Koehler, C. A., Paul, N. M., and De Haan, D. O.: Oligomer Formation in Evaporating Aqueous Glyoxal and Methyl Glyoxal Solutions, Environ. Sci. Technol., 40, 6318–6323, https://doi.org/10.1021/es060810w, 2006.

Matsunaga, S., Mochida, M., and Kawamura, K.: High abundance of gaseous and particulate 4-oxopentanal in the forestal atmosphere, Chemosphere, 55, 1143–1147, https://doi.org/10.1016/j.chemosphere.2003.10.004, 2004.

Maxut, A.: Formation mechanisms and yields of small imidazoles from reactions of glyoxal with NH4+ in water at neutral pH, 9, 2015.

McNeill, V. F.: Aqueous Organic Chemistry in the Atmosphere: Sources and Chemical Processing of Organic Aerosols, Environ. Sci. Technol., 49, 1237–1244, https://doi.org/10.1021/es5043707, 2015.

Müller, M., Anderson, B. E., Beyersdorf, A. J., Crawford, J. H., Diskin, G. S., Eichler, P., Fried, A., Keutsch, F. N., Mikoviny, T., Thornhill, K. L., Walega, J. G., Weinheimer, A. J., Yang, M., Yokelson, R. J., and Wisthaler, A.: In situ measurements and modeling of reactive trace gases in a small biomass burning plume, Atmos. Chem. Phys., 16, 3813–3824, https://doi.org/10.5194/acp-16-3813-2016, 2016.

Newland, M. J., Rea, G. J., Thüner, L. P., Henderson, A. P., Golding, B. T., Rickard, A. R., Barnes, I., and Wenger, J.: Photochemistry of 2-butenedial and 4-oxo-2-pentenal under atmospheric boundary layer conditions, Phys. Chem. Chem. Phys., 21, 1160–1171, https://doi.org/10.1039/C8CP06437G, 2019.

Nozière, B., Dziedzic, P., and Córdova, A.: Formation of secondary light-absorbing "fulvic-like" oligomers: A common process in aqueous and ionic atmospheric particles?, Geophys. Res. Lett., 34, L21812, https://doi.org/10.1029/2007GL031300, 2007.

Nozière, B., Dziedzic, P., and Córdova, A.: Products and Kinetics of the Liquid-Phase Reaction of Glyoxal Catalyzed by Ammonium Ions (NH$_4^+$), J. Phys. Chem. A, 113, 231–237, https://doi.org/10.1021/jp8078293, 2009.

Obermeyer, G., Aschmann, S. M., Atkinson, R., and Arey, J.: Carbonyl atmospheric reaction products of aromatic hydrocarbons in ambient air, Atmospheric Environment, 43, 3736–3744, https://doi.org/10.1016/j.atmosenv.2009.04.015, 2009.

580 Pöschl, U.: Atmospheric Aerosols: Composition, Transformation, Climate and Health Effects, Angew. Chem. Int. Ed., 44, 7520–7540, https://doi.org/10.1002/anie.200501122, 2005.

Powelson, M. H., Espelien, B. M., Hawkins, L. N., Galloway, M. M., and De Haan, D. O.: Brown Carbon Formation by Aqueous-Phase Carbonyl Compound Reactions with Amines and Ammonium Sulfate, Environ. Sci. Technol., 48, 985–993, https://doi.org/10.1021/es4038325, 2014.

585 Raoult, S., Rayez, M.-T., Rayez, J.-C., and Lesclaux, R.: Gas phase oxidation of benzene: Kinetics, thermochemistry and mechanism of initial steps, Phys. Chem. Chem. Phys., 6, 2245, https://doi.org/10.1039/b315953a, 2004.

Saleh, R.: From Measurements to Models: Toward Accurate Representation of Brown Carbon in Climate Calculations, Curr Pollution Rep, 6, 90–104, https://doi.org/10.1007/s40726-020-00139-3, 2020.

Sareen, N., Schwier, A. N., Shapiro, E. L., Mitroo, D., and McNeill, V. F.: Secondary organic material formed by
590 methylglyoxal in aqueous aerosol mimics, Atmos. Chem. Phys., 10, 997–1016, https://doi.org/10.5194/acp-10-997-2010, 2010.

Sedehi, N., Takano, H., Blasic, V. A., Sullivan, K. A., and De Haan, D. O.: Temperature- and pH-dependent aqueous-phase kinetics of the reactions of glyoxal and methylglyoxal with atmospheric amines and ammonium sulfate, Atmospheric Environment, 77, 656–663, https://doi.org/10.1016/j.atmosenv.2013.05.070, 2013.

595 Seinfeld, J. H. and Pandis, S. N.: Atmospheric Chemistry and Physics: From Air Pollution to Climate Change, John Wiley & Sons, Incorporated, New York, 2016.

Shapiro, E. L., Szprengiel, J., Sareen, N., Jen, C. N., Giordano, M. R., and McNeill, V. F.: Light-absorbing secondary organic material formed by glyoxal in aqueous aerosol mimics, 12, 2009.

Smith, D. F., Kleindienst, T. E., and McIver, C. D.: Primary Product Distributions from the Reaction of OH with m-, p-Xylene,
600 1,2,4- and 1,3,5-Trimethylbenzene, Journal of Atmospheric Chemistry, 34, 339–364, https://doi.org/10.1023/A:1006277328628, 1999.

Stockwell, C. E., Veres, P. R., Williams, J., and Yokelson, R. J.: Characterization of biomass burning emissions from cooking fires, peat, crop residue, and other fuels with high-resolution proton-transfer-reaction time-of-flight mass spectrometry, Atmos. Chem. Phys., 15, 845–865, https://doi.org/10.5194/acp-15-845-2015, 2015.

605 Strollo, C. M. and Ziemann, P. J.: Products and mechanism of secondary organic aerosol formation from the reaction of 3-methylfuran with OH radicals in the presence of NOx, Atmospheric Environment, 77, 534–543, https://doi.org/10.1016/j.atmosenv.2013.05.033, 2013.

Tao, W., Su, H., Zheng, G., Wang, J., Wei, C., Liu, L., Ma, N., Li, M., Zhang, Q., Pöschl, U., and Cheng, Y.: Aerosol pH and chemical regimes of sulfate formation in aerosol water during winter haze in the North China Plain, Atmos. Chem. Phys., 20,
610 11729–11746, https://doi.org/10.5194/acp-20-11729-2020, 2020.

Volkamer, R., Platt, U., and Wirtz, K.: Primary and Secondary Glyoxal Formation from Aromatics: Experimental Evidence for the Bicycloalkyl−Radical Pathway from Benzene, Toluene, and p -Xylene, J. Phys. Chem. A, 105, 7865–7874, https://doi.org/10.1021/jp010152w, 2001.

Volkamer, R., San Martini, F., Molina, L. T., Salcedo, D., Jimenez, J. L., and Molina, M. J.: A missing sink for gas-phase
615 glyoxal in Mexico City: Formation of secondary organic aerosol, Geophys. Res. Lett., 34, L19807, https://doi.org/10.1029/2007GL030752, 2007.

Wang, C., Lei, Y. D., Endo, S., and Wania, F.: Measuring and Modeling the Salting-out Effect in Ammonium Sulfate Solutions, Environ. Sci. Technol., 48, 13238–13245, https://doi.org/10.1021/es5035602, 2014.

Waxman, E. M., Elm, J., Kurtén, T., Mikkelsen, K. V., Ziemann, P. J., and Volkamer, R.: Glyoxal and Methylglyoxal Setschenow Salting Constants in Sulfate, Nitrate, and Chloride Solutions: Measurements and Gibbs Energies, Environ. Sci. Technol., 49, 11500–11508, https://doi.org/10.1021/acs.est.5b02782, 2015.

Yan, X., Bain, R. M., and Cooks, R. G.: Organic Reactions in Microdroplets: Reaction Acceleration Revealed by Mass Spectrometry, Angew. Chem. Int. Ed., 55, 12960–12972, https://doi.org/10.1002/anie.201602270, 2016.

Yu, G., Bayer, A. R., Galloway, M. M., Korshavn, K. J., Fry, C. G., and Keutsch, F. N.: Glyoxal in Aqueous Ammonium Sulfate Solutions: Products, Kinetics and Hydration Effects, Environ. Sci. Technol., 45, 6336–6342, https://doi.org/10.1021/es200989n, 2011.

Yuan, Y., Zhao, X., Wang, S., and Wang, L.: Atmospheric Oxidation of Furan and Methyl-Substituted Furans Initiated by Hydroxyl Radicals, J. Phys. Chem. A, 121, 9306–9319, https://doi.org/10.1021/acs.jpca.7b09741, 2017.

Zhang, Y., Dore, A. J., Ma, L., Liu, X. J., Ma, W. Q., Cape, J. N., and Zhang, F. S.: Agricultural ammonia emissions inventory and spatial distribution in the North China Plain, 158, 490–501, https://doi.org/10.1016/j.envpol.2009.08.033, 2010.

Table 1: List of experiments performed, according to reaction. pH ranges and initial butenedial (BD) and NH_X concentrations are provided.

Reaction	$[BD]_0$ (M)	$[NH_X]_0$ (M)	pH
BD/H_2O	0.029-0.55	0	3
BD/OH^-	0.2-0.3	0	8.8-10.4
BD/NH_X	0.4-0.9	0.2-0.9	3.6-8.8

Table 2: Butenedial/OH^- reaction, kinetic expression of the rate law, and corresponding estimates of the coefficients in the rate constant and their standard errors. a_I and a_{III} are well constrained. Although a_{II} has a large standard error, it appears to not severely impact agreement between model and measurement (Figure 3). See Equation 1 for the expression of k_1 in terms of its coefficients, a_I, a_{II}, and a_{III}, and OH^-.

	Reaction	Kinetic expression	Estimated coefficients
(R1)	[structure] + OH^- → accretion product	k_1 [BD]	$a_I = 15.5 \pm 0.869$ $M^{-1} \cdot s^{-1}$, $a_{II} = 64.6 \pm 4.00 \times 10^3$ M^{-2} s^{-1}, $a_{III} = 1.61 \times 10^4 \pm 2.43 \times 10^3$ M^{-1}
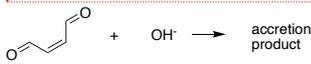
Table 3: Reactions in the butenedial/NH_X model kinetic mechanism, their rate laws as expressed in the mechanism, and corresponding estimates of the rate constants and their standard errors.

	Reaction	Kinetic expression	Estimated rate constant
(R2)	[structure] + NH_3 → [structure] + H_2O	k_2 [BD] [NH_3]	25.1 ± 3.72 M^{-1} min^{-1}
(R3)	[structure] + [structure] OH^-→ [structure]	k_3 [BD] [PR] [OH^-]	$6.36 \times 10^6 \pm 1.94 \times 10^6$ M^{-2} min^{-1}
(R4)	[structure] + accretion product → accretion product	k_4 [BD] [AP]	$0.255 \pm 1.80 \times 10^{-2}$ M^{-1} min^{-1}
(R5)	[structure] + accretion product → accretion product	k_5 [PR] [AP]	$0.460 \pm 3.98 \times 10^{-2}$ M^{-1} min^{-1}
(R6)	[structure] + accretion product → accretion product	k_6 [BD-PR] [AP]	$0.172 \pm 2.18 \times 10^{-2}$ M^{-1} min^{-1}
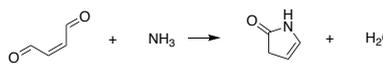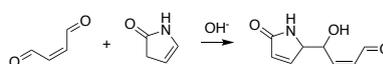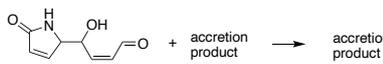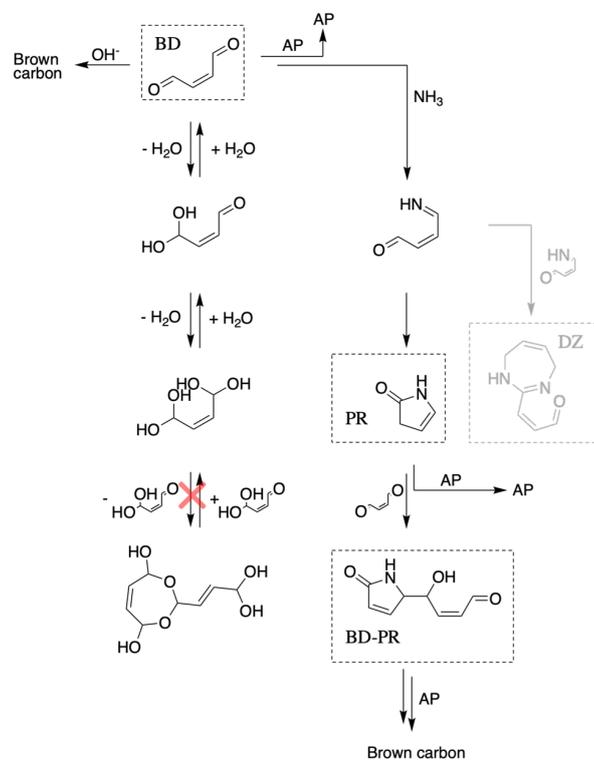
Figure 1: This chemical scheme is proposed for butenedial reactivity in an aqueous solution with NH_X. Reactions that are grayed out were not explicitly included in the model kinetic mechanism. Butenedial/OH⁻ and butenedial/NH₃ reactions lead to brown carbon formation through accretion reactions. Accretion reactions with reactants, products, and accretion products (AP) are observed in the butenedial/NH₃ pathway. Acetal oligomer formation is not observed.

650
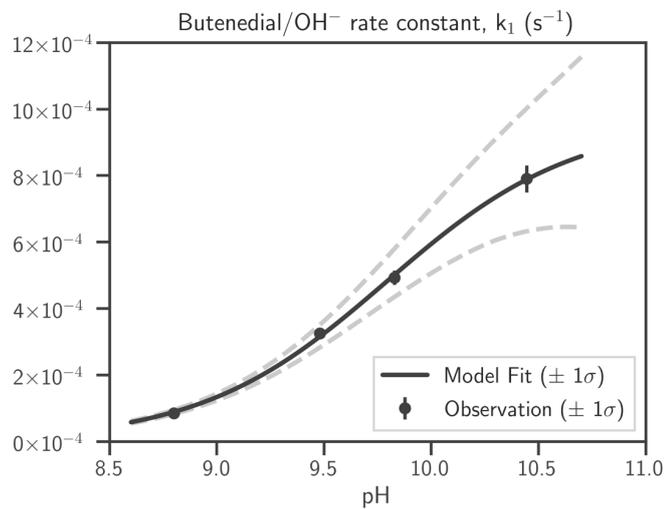
Figure 2: The butenedial/OH⁻ rate constant versus pH is shown. Observed k_1 are from kinetic fits to butenedial decay measured through four BD/OH⁻ experiments each held at constant pH. A fit to the empirical formulation of Fratzke et al. (1986) shows good agreement for all observations.

655
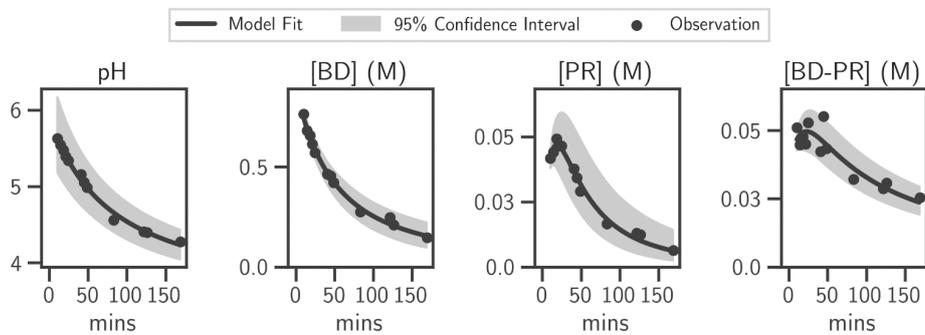
Figure 3: Comparison of measurement and model fit of 0.9 M BD/0.9 M NH$_X$ solution. Butenedial/NH$_X$ model kinetic mechanism was fit to measurements of this solution. The output (best model fit and 95% confidence interval) and observations are shown for all modeled species. NH$_X$ was not measured explicitly but was assumed to be consumed at a 1:1 ratio with butenedial. pH was estimated empirically outside of the model fit. Only the best model fit of pH was taken as input into the model kinetic mechanism, although the 95% confidence interval is reported for the empirical fitting of pH.

660
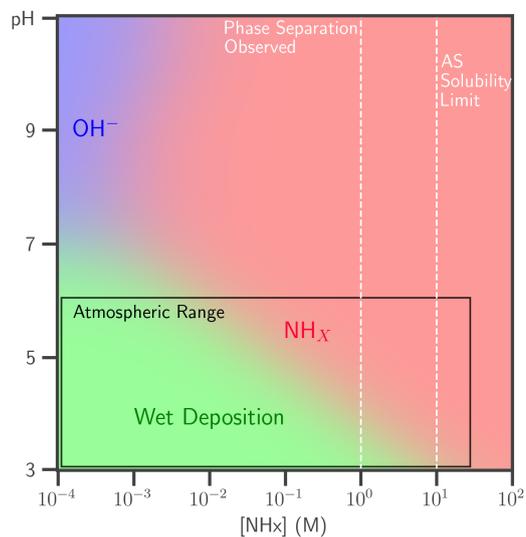
Figure 4: The dominant butenedial loss pathway, reaction with OH⁻ (blue) or NH$_X$ (red) and wet deposition (green), is shown as a function of pH and NH$_X$. AS is the NH$_X$ source. Loss via wet deposition is considered to have a one-week lifetime, typical of atmospheric particles. The range of pH (3-6) and NH$_X$ concentration (<28 M) relevant to the atmosphere is overlaid on the plot, as well as the NH$_X$ concentrations at which phase separation in the mixtures was observed and the AS solubility limit.